ACI STRUCTURAL JOURNAL

A JOURNAL OF THE AMERICAN CONCRETE INSTITUTE

Prepublished Paper

This is a prepublished manuscript. The final manuscript is tentatively scheduled for V. 121, No. 5 and is subject to change.

The DOI for this paper is 10.14359/51740864 and will not change, but won't be activated until the issue has been published.

American Concrete Institute

Thermomechanical Hysteresis of RC Beams Retrofitted with CFRP and UHPC

Yail J. Kim and Ibrahim Bumadian

Yail J. Kim, FACI, is President of the Bridge Engineering Institute, An International Technical Society, and a Professor in the Department of Civil Engineering at the University of Colorado Denver, Denver, CO. He is Chair of ACI Subcommittee 440I (FRP-Prestressed Concrete) and past Chair of ACI Committee 345 (Concrete Bridge Construction and Preservation). He is a member of ACI Committees 342 (Evaluation of Concrete Bridges and Bridge Elements), 440 (Fiber Reinforced Polymer Reinforcement), and Joint ACI-ASCE Committee 343 (Concrete Bridge Design). He is the recipient of the Chester Paul Siess Award for Excellence in Structural Research in 2019. His research interests encompass advanced composite materials for rehabilitation, structural informatics, complex systems, and science-based structural engineering, including statistical, interfacial, and quantum physics.

Ibrahim Bumadian is a PhD Student in the Department of Civil Engineering at the University of Colorado Denver, where he received an MS in civil engineering in 2014. His research interests include the behavior of constructed structures in corrosive service conditions and the implications of multi-hazard.

Abstract: This paper presents the behavior of reinforced concrete beams retrofitted with carbon fiber reinforced polymer (CFRP) sheets and ultra-high performance concrete (UHPC) jackets in a multihazard environment. Following the procedural protocol of a published standard, the beams are cyclically loaded under thermomechanical distress at elevated temperatures, varying from 25°C (77°F) to 175°C (347°F), in order to examine their hysteretic responses alongside ancillary testing. The thermal conductivity of UHPC is higher than that of ordinary concrete by more than 62% and, according to a theoretical inference, premature delamination would not occur within the foregoing temperature range. The difference of load-carrying capacities between the strengthened and unstrengthened beams declines with temperature. While the UHPC+CFRP retrofit scheme is beneficial, CFRP plays a major role in upgrading the flexural resistance. The thermomechanical loading deteriorates the hysteretic loops of the beams, thereby lowering the stiffness and capacity. Elevated temperatures are concerned with the pinching, plasticity, characteristic rigidity, stress redistributions, and energy-release patterns of the beams. Due to the retrofit, the configuration of plastic hinges alters and the localized sectional deformations form a narrow damage zone. The adverse effects of the temperatures on rotational stiffness are pronounced during the early loading stage of the beams.

Keywords: carbon fiber reinforced polymer (CFRP); hysteresis; retrofit, strengthening, thermomechanical loading

INTRODUCTION

Multihazards are not part of most seismic design specifications. For instance, the ASCE/SEI 43 Standard[1] offers four limit-state criteria solely based on structural deformations in line with response spectrum parameters. Precedent research claims that seismic vulnerability increases significantly when incorporating secondary loadings like tsunami[2], flood[3], wind[4], scour[5], and fire[6]. Traditional approaches separately treat structural loads without integrating individual actions[7]; as a result, disastrous incidents that were unexpected during the design procedure may arise[8]. A case study on the 2004 Indian Ocean catastrophe, where earthquake-wave-combined loadings brought about massive destruction of buildings, recommends that multihazards be explicitly allowed for in designing critical structures[9].

Seismic deficiency is a ubiquitous challenge facing the built-environment community and an annual budget of $6.1 billion is estimated to cope with earthquake risks for the U.S. building stock[10]. Inappropriately detailed structures undergo flawed energy dissipation appertaining to capacity reductions and pinched hysteresis loops[11]. Instead of replacement that necessitates unaffordable resources and societal costs, owners prefer conducting repairs and renovations[12]. Whereas state-of-the-art papers promote the positive impact of various techniques[13,14], practical issues are often acknowledged in established methods: magnified self-weight, escalated sectional geometries, modified stiffness, intensive labor, and prolonged downtime[14,15]. Furthermore, upgrading substandard structures is correlated with large uncertainties and incurs financial expenditure[16,17]. Rehabilitation methodologies should, thus, be selected rigorously.

Composite materials are receiving special attention for retrofitting deficient concrete members, such as ultra-high performance concrete (UHPC) and carbon fiber reinforced polymer (CFRP)[18,19]. The high compressive strength of UHPC, over f'_c = 120 MPa (17 ksi), provides the

means to reduce architectural dimensions required for ordinary concrete with remarkable durability[20,21]. Experimental investigations report that UHPC-jacketing improved the axial/flexural capacities of building elements and relieved brittle failure under cyclic loading[22,23]. Likewise, CFRP-confinement furnishes several advantages, namely, enhanced rotational resistance, mitigated concrete-splitting, restricted rebar-buckling, morphological adaptability, compliance with published standards, and broad coverage from component to system levels[24]. Members retrofitted with CFRP are, however, intrinsically vulnerable to temperature-induced distress because the performance of the strengthening system is reliant upon polymeric adhesives[25]. Such a situation is instantiated by an earthquake that prompts fires alongside the continued displacement reversals of strengthened members resulting from main- and after-shocks[26-28]. Despite the significance of thermomechanical loadings, specific information is not stipulated in existing design guidelines with regard to externally bonded CFRP sheets[24,29], which warrants sophisticated research for the advancement of current knowledge. In addition, a new opportunity may be created by coupling these proven materials for multihazard application.

This paper explores the behavior of reinforced concrete beams retrofitted with CFRP and UHPC subjected to simulated earthquake drifts at elevated temperatures. The objective of the present experimental study is twofold: i) to explicate the undiscovered failure mechanism of CFRP-strengthened beams under concurrent thermomechanical loadings and ii) to ascertain the potential of a rehabilitation method comprising UHPC jackets layered with CFRP sheets. Hysteretic responses, performance degradation, and inelastic deformations are expounded for the sake of understanding the retrofit systems' functionality in the aggressive loading environments.

RESEARCH SIGNIFICANCE

Multihazard design is an emerging concept that can address complex interactions and cumulative demands concerning the operational safety of structures[7]. The outcomes of multihazard loadings are dissimilar to those of respective ones; accordingly, arithmetic sums in each load deviate from actual effects[30]. Notwithstanding the broad adoption of non-conventional materials for strengthening concrete structures, the behavior of members with these materials under thermal and cyclic loadings is not well elucidated yet. In light of this, there are practical needs to evaluate the response of retrofitted members simultaneously exposed to earthquakes and elevated temperatures, which is not an uncommon scenario during a seismic event[31]. Attempts are made to document the ramifications of thermomechanical loadings for the seismic performance of cantilevered beams retrofitted with CFRP and UHPC+CFRP systems.

EXPERIMENTAL PROCEDURE

Commensurate with the aim of the aforementioned research program, laboratory testing is performed to examine the synergistic implications of thermal and cyclic loadings for the behavior of cantilever beams strengthened with CFRP and UHPC. Outlined below are descriptions on materials, specimens, strengthening details, and a loading protocol.

Materials

Concrete was mixed to accomplish a specified strength of 25 MPa (3,630 psi) in compression (mix ratio of water:cement:sand:gravel = 1:1.9:5.1:7.3 by weight). After 28 days of curing in a moisture-controlled chamber (a 99% humidity at 23°C (73°F)), cylinders were tested in accordance with ASTM C39[32] and an average strength of f'_c = 24.9 MPa (3,610 psi) was obtained. Steel bars with a yield strength of f_y = 414 MPa (60 ksi) and 250 MPa (36 ksi)) were used for flexural and shear reinforcement (No. 3 (9.53 mm (0.375 in.) in diameter) and No. 2

(6.35 mm (0.25 in.) in diameter), respectively) in order to accommodate practical aspects in the field. Unidirectional CFRP composite sheets, consisting of dry carbon fabrics impregnated in a two-part epoxy resin, required a curing time of seven days at room temperature for the succeeding properties based on an equivalent fiber thickness of t_f = 0.165 mm (0.0065 in.): tensile strength (f_{fu}) = 3,800 MPa (550 ksi), elastic modulus (E_f) = 227 GPa (33,000 ksi), ultimate strain (ε_{fu}) = 0.0167, and glass transition temperature (T_g) = 71°C (163°F). The epoxy that was mixed with a resin and a hardener at a mass ratio of 3:1 possessed a tensile strength of f_{epu} = 55 MPa (8,000 psi) with an elastic modulus of E_{ep} = 3 GPa (440 ksi). The coefficient of thermal expansion of the CFRP and epoxy was $\alpha_f = -0.38 \times 10^{-6}$/°C ($-0.21 \times 10^{-6}$/°F) and $\alpha_{ep} = 35 \times 10^{-6}$/°C ($20 \times 10^{-6}$/°F), respectively. A commercial UHPC product was employed and its guaranteed properties are: compressive strength ($f_{c\text{-}UHPC}$) = 120 MPa (17.4 ksi), flexural strength ($f_{r\text{-}UHPC}$) = 14 MPa (2,030 psi), elastic modulus (E_{UHPC}) = 30 GPa (4,350 ksi), shrinkage < 0.01%, and ASTM-C-230 flow = 280 mm (11 in.).

Specimens

As depicted in Fig. 1(a), concrete beams were cast with a dimension of 100 mm (4 in.) by 165 mm (6.5 in.) by 1,200 mm (3.9 ft). Two No. 3 bars were longitudinally placed at an effective depth of 135 mm (5.3 in.) and multiple No. 2 bars were arranged at spacings of 75 mm (3 in.). To resist negative bending, compression rebars were extended to the mid-length of the beams.

Retrofit

Strengthening work was undertaken for upgrading the seismic performance of the beams, which would be tested under a cantilever condition. To determine the zone of retrofit, a plastic hinge length was calculated as per ACI 440.2R-17[24] and rounded to be 350 mm (13.8 in.) for practical convenience. Two retrofit strategies were implemented with CFRP and UHPC+CFRP. The first

scheme involved the complete wrapping of the critical region using the CFRP sheets (Fig. 1(b)). After roughening the target concrete surface with an electric steel-wire brush, the blended epoxy was applied and single-layer carbon fabrics were impregnated as part of a wet-layup process. The orientation of the fibers was perpendicular to the longitudinal rebars. The composite system was then cured for seven days at room temperature. For the second scheme, a UHPC jacket was added (Fig. 1(c)) and the CFRP sheets fully enclosed the 28-day cured jacket. Table 1 summarizes the identification of these retrofitted beams together with loading schemes; namely, the first letter denotes a loading type (*M* = monotonic and *C* = cyclic), the second component pertains to elevated temperatures in degrees Celsius, and the last part manifests the type of strengthening (NO = unstrengthened, *CF* = CFRP, and *UC* = UHPC+CFRP).

Testing

Ancillary tests—To attain the thermal conductivity (*K*) of the ordinary concrete and UHPC mixtures, a non-contacting thermometer was utilized (Fig. 2(a): a concrete disk was placed on the electric apparatus and the progression of heat was measured by a non-contacting thermometer)

$$K = \frac{Qd}{A\Delta T} \quad (1)$$

where Q is the supplied heat energy (Q = 3 W (10.2 BTU/hr)); d and A are, respectively, the depth and cross-sectional area of the specimen (d = 0.08 m (3.15 in.) and A = 0.002 m^2 (3 $in.^2$)); and ΔT is the difference in temperature. The physical significance of measuring the thermal conductivity is that it dominates the formation of temperature gradients, thereby affecting the thermal strains of the ordinary concrete and UHPC (the conductivity of thin CFRP composites is negligible relative to that of concrete[33]). A thermal camera monitored the temperature variation of the concrete specimens for infrared thermography. The camera, built upon the multi-spectral

dynamic imaging technology, generated images at a resolution of 19,200 pixels with a sensitivity of less than 0.06°C (0.11°F) and a frame rate of 9 Hz[34]. The frequency of temperature-sampling was every 5 min. for a period of 3 hrs, which was sufficient to cover structural examinations (to be described), and the test was replicated 3 times.

Thermomechanical loading—all beams were cantilevered with a custom-made fixture and the distance from the fixed end to the center of the loading bracket was 700 mm (27.5 in.), as shown in Figs. 2(b) and (c). The fixture was composed of two hollow steel sections (100 mm (4 in.) wide by 100 mm (4 in.) deep by 16 mm (0.625 in.) thick), ASTM A325 threaded steel rods (16 mm (0.63 in.) in diameter), and a rigid support that was anchored to the strong floor. The portion of each beam, embedded in the fixture with a length of 300 mm (11.8 in.), was confined by the CFRP sheets to preclude premature failure. For the application of heat, the retrofitted part of the beams was wrapped with a glass-reinforced silicon rubber pad and steel wires (Fig. 2(c)). The pad was electrically powered and perfluoroalkoxy lead wires generated thermal energy: this system is frequently used to simulate heat transfer in laboratory research[35,36]. Given that the temperatures of insulated CFRP-strengthened members subjected to a fire are below 150°C (302°F) over an exposure period of 2 to 3 hrs on many occasions[37,38], the investigation range of the present study was set from 25°C (77°F) to 175°C (347°F) with an assumption that the members were adequately insulated. The preset temperature of the heating pad was automatically adjusted by a digital controller (Fig. 2(c), inset). Subsequently, the prepared beams were loaded mechanically and thermomechanically (Figs. 2(b) and (c), respectively) in conformity with the loading protocol of FEMA 461[39] (Fig. 2(d)). It should be noted that the beams cyclically loaded without thermal distress (C25CF and C25UC) can represent situations where an earthquake-

induced fire does not break out; on the contrary, other beams (C75CF to C175CF and C75UC to C175UC) encompass instances with combined load scenarios.

Instrumentation—A load cell and a displacement sensor, which were built in the servo-actuator unit, recorded the behavior of the test beams. Temperatures on the surface of CFRP (inside the heating pad) were logged by thermocouple wires. A preheating period of 10 min. was required for all thermomechanically loaded beams and the target temperatures were maintained until the beams failed (Fig. 2(e)).

RESULTS AND DISCUSSION

Diverse technical aspects are expatiated from material and structural points of view to comprehend the performance of retrofitted cantilever beams subjected to thermomechanical loadings. Emphasis is placed on the thermal properties of ordinary concrete and UHPC, as well as their conceptual performance reliability, and on the hysteretic responses and flexural characteristics of the beams.

Thermal Conduction

The thermometer-measured conductivities of the concrete specimens are shown in Figs. 3(a) and (b). Also shown are comparative plots against the conductivities quantified by the infrared spectroscopy. While the thermal response of the ordinary concrete was consistent (coefficient of variation = 0.05, Fig. 3(a)), that of UHPC was somewhat irregular (coefficient of variation = 0.12, Fig. 3(b)). This observation is explained by their different mineralogical compositions: the crystallinity of densely packed quartz sands in the UHPC mixture enabled a rapid flux of heat in multiple directions[40]. The average conductivity of UHPC was higher by up to 62.9% relative to the case of the ordinary concrete (Fig. 3(c)), which aligns with the fact that the vulnerability of high-strength concrete to a fire (thermal spalling) is higher than its low-strength counterpart[41].

With a consideration that heat currents in materials sharing contact surfaces are equal[42], the conductivity test results were utilized to estimate temperatures at the interface between the beam concrete and UHPC (Fig. 1(c))

$$T_{interface} = \frac{\alpha T_{applied} + T_0}{1+\alpha} \quad (2)$$

$$\alpha = \frac{K_{UHPC} t_{concrete}}{K_{concrete} t_{UHPC}} \quad (3)$$

where $T_{interface}$ is the interface temperature; $T_{applied}$ and T_0 are the applied and initial temperatures of the beam system, respectively (T_0 in the beam concrete was assumed 25°C (77°F)); $t_{concrete}$ and t_{UHPC} are the thickness of the ordinary concrete and UHPC, respectively (for demonstration purposes, $t_{concrete}$ = 82.5 mm (3.25 in.) and t_{UHPC} = 30 mm (1.2 in.) were used, Fig. 1(c)). When the applied temperature was increased, the ratio of $T_{interface}$ to $T_{applied}$ dwindled and stabilized (Fig. 3(d)). Therefore, practically speaking, the proposed UHPC-retrofit system would not experience premature delamination as long as the beam is properly insulated: previous research[43] reports that interfacial deterioration can take place between ordinary concrete and UHPC at a temperature above 300°C (572°F).

Suitability of UHPC as a Retrofit Material

The amount of disorder in the concrete composition was appraised by the change of entropy (ΔS)

$$\Delta S = \frac{Q}{\left(1/T_L - 1/T_H\right)} \quad (4)$$

where T_L and T_H are the temperatures at the top and bottom of the specimen (Fig. 2(a)), respectively. In statistical physics[44], entropy is regarded as a representative metric to figure out the degree of randomness in a system (tantamount to disorder). The entropy change of the concrete mixtures precipitously rose, when the heat energy was applied, and ebbed with time

(Fig. 4(a)). The positive values of the entropy ($\Delta S > 0$) impart that the elevated temperatures incurred an irreversible process in the mixtures[45], including chemical and physical alterations in the microstructures[46]. The ordinary concrete reacted more quickly than UHPC, meaning that the composition of the ordinary concrete possessed a higher likelihood for variability in terms of material stability. Examples can be found in literature[47]: compared with UHPC, the compressive strength and bond of ordinary concrete degrade swiftly in aggressive environments. The development of entropy is portrayed in Fig. 4(b). Even if the tangent of the ordinary concrete's curve was remarkably stiff within a time period between 0 min. and 25 min., the difference against the tangent of UHPC disappeared after 100 min. Part of water in the mixtures commenced to release and evaporate when the applied temperature exceeded 100°C (212°F), as marked in Fig. 4(b), which is believed to be a driving force for making the internal composition of the mixtures stable through a phase transformation[48,49]. Contemplating the equivalence of entropy and uncertainty[50], the low-entropy UHPC was notionally confirmed as a suitable material for upgrading existing structural members with high reliability.

Load-Bearing Capacity

Figure 5 exhibits the flexural capacity of the test beams. The capacities of the CF and UC series under the cyclic loading without thermal exposure (the absolute maximum values at 25°C (77°F) in Table 1) were 1.94 and 2.12 times higher than the capacity of the monotonically loaded unstrengthened control beam (Fig. 5(a)). With the increased temperature, the efficacy of the retrofit systems decreased by degrees and the capacity of the strengthened beams fell below the level of the unstrengthened beam at 175°C (347°F). Shown in Fig. 5(b) are the repercussions of the thermal distress for the capacity of the periodically loaded CF and UC beams. The heat-induced capacity reduction of the beams was prominent when the applied temperature went over

the glass transition temperature of the epoxy resin ($T_{applied} > T_g$ = 71°C (163°F)). The almost identical reduction rates of the CF and UC beams imply that the CFRP sheets were the major constituent from a load-carrying standpoint; scilicet, the role of CFRP was greater than that of UHPC in resisting the sinusoidal mechanical load.

To further investigate the individual contribution of CFRP and UHPC under the cyclic load environment, the relative capacity of the strengthened beams at elevated temperatures ($\Delta P_{rc}(T)$) was extracted from the capacity of the unstrengthened beam tested at 25°C (77°F)

$$\Delta P_{rc}(T) = \frac{\left|P_{u-str.}(T)\right| - P_{u-unstr.}\left(25^{o}C\right)}{P_{u-unstr.}\left(25^{o}C\right)} \quad (5)$$

where $P_{u\text{-}str.}(T)$ and $P_{u\text{-}unstr.}(25^{o}C)$ are the capacities of the strengthened and unstrengthened beams at a temperature T and 25°C (77°F), respectively. As graphed in Fig. 5(c), the effects of the retrofit elements were clearly distinguishable. The synergistic combination of UHPC and CFRP better raised the beams' capacity in comparison with the case involving CFRP alone; nonetheless, the average fraction of UHPC was 8.8% in the increased capacity (Fig. 5(d)). This fact reaffirms that the CFRP confinement accounting for the rest (91.2%) was the primary component of the strength gain.

Flexural Behavior

Hysteresis of beams with CFRP—The load-deflection diagram of the CF series beams is described in Fig. 6. For reference purposes, the behavior of the monotonically loaded beams (M25NO and M25CF) is also visible in the inset of Fig. 6(a). The strengthened beam subjected to the mechanical loading at 25°C (77°F) revealed steady responses until the 26th cycle (Fig. 6(a)), after which a sudden increase in deflection was noted with successively decrementing post-peak loads. This was ascribed to the occurrence of local CFRP debonding in C25CF, which

267 was related to the wet-layup process that could entail nonuniform bond quality[51]. Besides, during
268 the course of increasing deflection amplitude in compliance with the FEMA's test protocol (Fig.
269 2(d)), the repeated slippage between the concrete substrate and CFRP caused internal friction
270 that exacerbated the amicable dissipation of excitation energy[52].

271 As shown in Fig. 6(b), the transmitted heat above the glass transition temperature of the
272 epoxy accelerated the synergistic degradation of the CFRP-strengthened beam; consequently, the
273 loading slope of the hysteretic loops gradually descended with the increased cycle. The
274 unloading curves of C75CF in the first and third quadrants were deemed elastic because the
275 reversal of the mechanical loading released the accumulated stresses of the beam; hence, the
276 post-peak slopes were nearly parallel to the pre-yield slopes. Unlike the occasion of C25CF, the
277 residual deflection of C75CF regularly developed with respect to the number of cycles (Fig. 6(b),
278 inset), indicating that the partly flawed wet-layup of the C25CF beam was merely an unintended
279 experimental fault.

280 When the applied temperature was increased to 125^{o}C (257^{o}F) and 175^{o}C (347^{o}F), the
281 influence of the thermomechanical distress became obvious (Figs. 6(c) and (d)). The thermally
282 weakened CFRP sheets combined with enlarged concrete cracks after yielding abated the load-
283 carrying ability of the beams. In addition, the pinching of the reciprocating curves, accompanied
284 by the softened slopes while the beams were loaded and unloaded (a schematic illustration is
285 available in Fig. 6(c)), was noticed. Specifically, the pinching effect was negligible prior to the
286 yielding of the rebars, whereas it was prominent in the post-yield domain of the hysteretic loop:
287 the response of the beams is given in the inset of Fig. 6(c) with normalized loads ($P/|P_{max}|$) at the
288 10th and 20th cycles. Given that the extent of pinching is governed by the progression of a

hysteretic slip[53], the thermomechanical loading was certainly responsible for expanding the interfacial dislocation of the CFRP-retrofit system.

Hysteresis of beams with UHPC and CFRP—Figure 7 displays the hysteretic behavior of the UC series beams. The stresses stemming from positive bending should be completely lost when a load reversal commenced for negative bending. However, such an ideal circumstance was not seen due to the growth of internal damage in the load-bearing system. The stiffness of C25UC was retained until the 24th cycle; then, a reduction in the slope was observed with a considerable increase in the deflection (Fig. 7(a)). Passing through the surged deflection at the 32nd cycle, the beam failed with localized damage outside the retrofitted zone (to be elaborated). When the thermal loading was applied, the pinched hysteresis loop of the UC beam became conspicuous (Fig. 7(b)): the loops of C25UC and C75UC are compared at the 32nd cycle in the inset of Fig. 7(b). This fact substantiates that significant plasticity arose in the retrofit system owing to the elevated temperature. Comprehensive discussions on the relationship between pinching and plasticity are found elsewhere[54].

As the temperature was raised over 125^{o}C (257^{o}F), the configuration of the hysteretic loops altered in the positive and negative loading directions (Figs. 7(c) and (d)). The so-called Bauschinger effect can account for this shifting of the loops from the third to the first quadrants in C125UC and C175UC. According to the Bauschinger mechanism[55], the cyclic thermomechanical loading redistributed the internal stresses of the beams and cumulatively dislocated their constituents in conjunction with strain hardening at every load reversal. The degree of damage accrual during the loading process was a function of the thermal exposure as well. The backbone curve of C175UC began to bifurcate from the curve of C125UC at 5 kN (1.1 kips) and the former's response slope was consistently lower than the slope of the latter (Fig.

7(d), inset). The softening of the backbone curve is a clear indication for the unfavorable evolution of plastic damage in the microstructures of the beam concrete and the retrofit elements, which provoked non-homogeneous deformations[56].

Bending Characteristics

The characteristic flexural rigidity of the unstrengthened and strengthened beams under the monotonic loading (M25NO and M25CF, respectively) is provided in Fig. 8(a). The characteristic rigidity (EI_{ch}) of the cantilever beams derived from their secant stiffness (Fig. 8(a), inset) was calculated semi-empirically by

$$EI_{ch} = \frac{\left|P_{i\max} L^3\right|}{3\delta_i} \tag{6}$$

where P_{imax} is the maximum load of the i^{th} cycle in either the positive or negative loading direction; δ_i is the deflection corresponding to P_{imax}; and L is the loading span. It is worth noting that the characteristic rigidity is intended to comparatively examine the performance of the test beams at elevated temperatures. The rigidity of M25CF was higher than that of M25NO, as shown in Fig. 8(a), except for the early loading stage where an abrupt increase in the deflection of M25CF took place at a load of 0.75 kN (0.17 kips) owing to the initial engaging of the beam with the fixture (Fig. 8(a), inset). The effectiveness of the retrofit systems subjected to the thermomechanical loading is studied in Fig. 8(b), where the characteristic rigidity of the CF and UC series beams at high temperatures was normalized by the rigidity at 25°C (77°F). The rigidity of both categories at their ultimate loads descended with temperature, corroborating the adverse thermal exposure in the matter of lowering the ability to resist bending. The slow reaction rate of the UC series against the CF series in Fig. 8(b) supports the efficaciousness of the UHPC jacket as a supplementary retrofit element.

Energy Dissipation

Figures 9(a) and (b) demonstrate the hysteretic energy of the CF and UC beams, respectively, that was dissipated with an increase in the loading cycle. The energy dissipation in this context corresponds to the release of strain energy stored in the beams when the mechanical loading was reversed: the area under the alternating loops in Figs. 6 and 7 was numerically integrated to obtain energy values. Aligning with repeated crack-opening-and-closing actions, the periodic iterations of the beams in the positive and negative directions led to the up and down trend of the energy curves. The amplification of the energy was marginal until the 23rd cycle; afterward, soaring spikes were recorded because of the enlarged inelastic deformation of the impaired concrete[57]. Moreover, the exponentially growing energy is attributed to the coalescence of micro-cracks that accrued during the preceding cycles and their unstable propagation[58]. Figure 9(c) plots the energy fraction of the test beams (the i^{th} cycle energy (E_i) divided by the maximum energy (E_{max}) of the respective beams). Contrary to the CF series (Fig. 9(c), inset), the development of the energy fraction in the UC series was dependent upon the thermomechanical cycles. It accords with previous research in that thermally deteriorated micro-pores can lower the fracture resistance of UHPC by partially decomposing C-S-H gels[59]; as a consequence, the amount of the dissipated energy increased at elevated temperatures. The energy release rate of selected beams (Figs. 9(a) and (b)) with respect to the mechanical cycle is graphically assessed in Fig. 9(d). The presence of heat changed the pattern of energy release in the CF beams (similar observations made for the UC beams were omitted due to the page limit). The abrupt release rate of the CF beam at 25^{o}C (77^{o}F) subsided as the temperature went up to 175^{o}C (347^{o}F); however, this temperature-sensitive rate was not contingent upon the retrofit scheme (Fig. 9(d), inset) for the reason that the softened CFRP sheets redistributed the applied mechanical stresses, as

discussed earlier, and the waned interface between the retrofit systems and the beams did not transfer the entire stresses owing to the loss of bond[60].

INELASTIC PERSPECTIVES

Three major facets associated with the post-yield behavior of the thermomechanically loaded beams are of interest: plastic hinges, deformation localization, and potential energy. These inelastic responses are a prerequisite for construing the near-failure state of the beams.

Formation of Plastic Hinges

Figure 10 pictures the typical failure mode of the unstrengthened and strengthened beams. Although the elastic moment of the cantilever was maximum at the fixed end, the flexural and flexure-shear cracks of the unstrengthened beam were 80 mm (3.1 in.) to 420 mm (16.5 in.) away from the support (Fig. 10(a)), where substantial rotations ensued to form a plastic hinge. Regarding the strengthened beams (Figs. 10(b) and (c)), concentrated cracking occurred immediately outside the retrofitted region and the longitudinal rebars did not buckle because of the closed stirrups (Fig. 10(b), inset). With the onset of steel-yielding, the plastic deformation of the cracked beams was aggravated, the width of the cracks widened, and finally the concrete spalled (Figs. 10(b) and (c)). The heated retrofit system preserved its conformational integrity under the incremental load reversals; as such, no visual damage was noticeable at the surface level.

Localized Deformation

A relationship between the thermal loading and the maximum deflection range (δ_{max}) of the strengthened beams is shown in Fig. 11(a). The declining propensity of the deflection range with temperature points out that the progressive breakdown of the interfacial bond in the retrofit system was influential on the translational response of the cantilevers under the displacement-

controlled loading condition. In other words, the heat energy degraded the structural adequacy of CFRP; accordingly, the ability to withstand the external excitation diminished alongside the reduced quantity of elastic recovery[61]. As charted in Fig. 11(b) where the drift ratio of the beams ($\lambda = \delta_{max}/L$) at 75°C (167°F) to 175°C (347°F) was normalized by that of the beams at 25°C (77°F), the drift ratio of the UC series was positioned below the ratio of the CF series because the UHPC jacket played a role as a stress-transfer medium between the concrete substrate and CFRP with retained adhesion at the elevated temperatures[62].

Figure 11(c) illustrates the effective curvature of the test beams (ψ) at failure

$$\psi = \frac{\left(\delta_{up}/L_{un} + \delta_{down}/L_{un}\right)}{L_{pe}} \quad (7)$$

where δ_{up} and δ_{down} are the upward and downward deflections of the beam, respectively ($\delta_{max} = \delta_{up} + \delta_{down}$); L_{un} is the length of the unstrengthened zone; and L_{pe} is the length of the effective plastic hinge (L_{pe} = 85 mm (3.35 in.) was measured, on average). In contrast with the conventional assumption on the rotation of a beam at the center of a plastic hinge ($L_p/2$)[63], the pivot of rotation in L_{pe} was right next to the CFRP termination where stresses were concentrated (Fig. 11(c), inset). The magnitude of the effective curvature was inversely proportional to the temperature (Fig. 11(c)): the deteriorated retrofit system alleviated the degree of bending so that the cantilever beams had a tendency to straighten with the lessened flexural rigidity. Additionally, the effective curvature of the beams was distributed under the thermomechanical loading (Fig. 11(d)). The importance of these curvature distributions is that the hinged region underwent appreciable deterioration, arising from the large inelastic deformations, and considerable strain energy was dissipated over the strengthened portion of the beams (L_{st}) subjected to the heat.

Potential Energy

The conformation of the cantilever may be idealized as a single-degree-of-freedom (SDOF) system with a rotational spring (Fig. 12(a)). This simplification cannot accurately reflect localized deformations in the vicinity of the CFRP termination; however, the SDOF representation is appropriate to holistically analyze the detrimental features of the thermomechanical loadings: the spring characterizes the total strain energy absorbed by the beam. The potential energy of the cantilever (Π) is expressed by

$$\Pi = \frac{1}{2}k\theta^2 - PL\sin\theta \tag{8}$$

where θ is the angle of rotation in radians and k is the rotational stiffness, which is attained from the equilibrium condition of Eq. 8 ($d\Pi/d\theta = 0$)

$$k = \frac{PL\cos\theta}{\theta} \tag{9}$$

When the angle of rotation ascended, the stiffness k went down asymptotically and the gap between the thermally conditioned and unconditioned cases decreased as well (Figs. 12(a) and (b)). These responses clarify that the influence of the heat-generated distress was more pronounced during the early stage of the mechanical loading ($\theta \leq 0.02$ radians). As far as the retrofit method is concerned, the UHPC jacket intensified the rotational stiffness regardless of temperature (Fig. 12(b), inset). Figure 12(c) shows the experimentally quantified potential energy of the beams. With the exception of C25CF suffering the wet-layup debonding, the potential energy of all other specimens rose in a linear manner up to failure. The temperature-dependent variation of the potential energy signifies that the thermal loading controlled the buildup of the internal strain energy linked with the work done by the mechanical load. Besides, the uncertain distinction of the maximum potential energy in the CF and UC series above 125^{o}C

(257°F) accentuates the reliance of the retrofit system on the performance of CFRP that was vulnerable to the high temperatures (Fig. 12(d)).

SUMMARY AND CONCLUSIONS

This paper has dealt with the thermomechanical behavior of reinforced concrete beams strengthened with CFRP sheets and UHPC jackets. The beams were cyclically tested in a cantilever condition as per the protocol of FEMA 461[39] at elevated temperatures varying from 25°C (77°F) to 175°C (347°F). After performing ancillary experiments, the hysteretic responses of the retrofitted beams were investigated with a focus on load-deflection relationships, flexural rigidity, energy dissipation, and inelastic failure states. The following are concluded.

- The thermal conductivity of UHPC was over 62% higher than the conductivity of the ordinary concrete. The predicted temperature variation at the interface between the ordinary concrete and UHPC indicated that premature delamination would not occur. The entropy-based inference of UHPC corroborated its adequacy as a retrofit material with low uncertainty.
- The superior load-carrying capacity of the retrofitted beams to that of the unstrengthened beam decreased when applied temperatures exceeded the glass transition temperature of the CFRP sheets. While the synergy of UHPC integrated with CFRP was apparent in flexural resistance, the contributive portion of UHPC and CFRP was 8.8% and 91.2%, respectively, on average.
- On the hysteretic behavior of the retrofitted beams, the thermomechanical loading degraded the stiffness and capacity. An obvious difference was noticed between the loading and unloading curves under cyclic load reversals, including damage propagation and stress release. Elevated temperatures raised the extent of pinching, especially in the

post-yield domain of the response loops, which signifies the developed plasticity and redistributed stresses of the load-bearing system.

- Although the characteristic rigidity of all strengthened beams declined owing to the thermal exposure, those with UHPC+CFRP outperformed their CFRP-only counterparts. The amount of energy dissipation leaped when the inelastic deformation of the beams went beyond a threshold limit. The applied heat altered the beams' energy release patterns from abrupt to gradual.
- The plastic hinge length of 350 mm (13.8 in.) calculated by ACI 440.2R-17[24] was reasonable for the unstrengthened cantilever showing a cracked region of 80 mm (3.1 in.) to 420 mm (16.5 in.) from the support. For the strengthened beams, the plastic hinge formed right outside the retrofit zone with an average pivot length of 85 mm (3.35 in.).
- As definitized by simplified single-degree-of-freedom cantilevers, the effects of the thermal distress on rotational stiffness were more detrimental during the early loading stage of the beams and the efficaciousness of UHPC was notable for intensifying the stiffness.

ACKNOWLEDGMENTS

The authors would like to acknowledge financial support from the U.S. Department of Transportation through the Mountain-Plains Consortium. Technical contents presented in this paper are based on the opinion of the authors, and do not necessarily represent that of others. Mr. P.W. Weber at ceEntek donated UHPC mixtures. Proprietary information is not provided to avoid commercialism.

REFERENCES

[1] ASCE. 2005. Seismic design criteria for structures, systems, and components in nuclear facilities (ASCE/SEI 43), American Society of Civil Engineers, Reston, VA.

[2] Huang, S. and Liu, C. 2023. A computational framework for fluid–structure interaction with applications on stability evaluation of breakwater under combined tsunami-earthquake activity, Computer-Aided Civil and Infrastructure Engineering, 38(3), 325-352.

[3] Argyroudis, S.A. and Mitoulis, S.A. 2021. Vulnerability of bridges to individual and multiple hazards- floods and earthquakes, Reliability Engineering & System Safety, 210, 107564.

[4] Li, C., Liu, Y., and Li, H.-N. 2021. Fragility assessment and optimum design of a steel-concrete frame structure with hybrid energy-dissipated devices under multi-hazards of earthquake and wind, Engineering Structures, 245, 112878.

[5] Badroddin, M. and Chen, Z. 2023. Probabilistic understanding of seismic performance of river-crossing bridges with scour effects: a Critical review and investigation of seismic-scour damage effects, International Journal of Civil Engineering, 21, 915-931.

[6] Kamalvand, M., Massumi, A., and Homami, P. 2023. Prediction of post-fire seismic performance of reinforced concrete frames, Structures, 56, 104874.

[7] Bruneau, M., Barbato, M., Padgett, J.E., Zaghi, A.E., Mitrani-Reiser, J., and Li, Y. 2017. State of the art of multihazard design, Journal of Structural Engineering, 143(10), 03117002.

[8] Hain, A., Zaghi, A., Padgett, J.E., and Tafur, A. 2023. Case studies of multihazard damage: Investigation of the interaction of Hurricane Maria and the January 2020 earthquake sequence in Puerto Rico, Frontiers in Built Environment, 9, 1128573.

[9] Ghobarah, A., Saatcioglu, M., and Nistor, I. 2006. The impact of the 26 December 2004 earthquake and tsunami on structures and infrastructure, Engineering Structures, 28, 312-326.

[10] FEMA. 2017. Hazus® estimated annualized earthquake losses for the United States (FEMA P-366), Federal Emergency Management Agency, Washington, D.C.

[11] Sengupta, P. and Li, B. 2014. Hysteresis behavior of reinforced concrete walls, Journal of Structural Engineering, 140(7), 04014030.

[12] Pohoryles, D.A., Bournas, D.A., Da Porto, F., Caprino, A., Santarsiero, G., Triantafillou, T. 2022. Integrated seismic and energy retrofitting of existing buildings: a state-of-the-art review, Journal of Building Engineering, 61, 105274.

[13] Cao, X.-Y., Shen, D., Feng, D.-C., Wang, C.-L., Qu, Z. and Wu, G. 2022. Seismic retrofitting of existing frame buildings through externally attached sub-structures: State of the art review and future perspectives, Journal of Building Engineering, 57, 104904.

[14] Echeverria, M.J., Mohammadgholibeyki, Negar, Liel, A.B., and Koliou, M. 2023. Achieving functional recovery through seismic retrofit of existing buildings: barriers and opportunities, Journal of Performance of Constructed Facilities, 37(4), 04023027.

[15] Engindeniz, M., Kahn, L. F., and Zureick, A.-H. 2005. Repair and strengthening of reinforced concrete beam-column joints: state of the art, ACI Structural Journal, 102(2), 187-197.

[16] Williams, M.S. and Sexsmith, R.G. 1995. Seismic damage indices for concrete structures: a state-of-the-art review, Earthquake Spectra, 11(2), 319-349.

[17] Ying, F.J., Wilkinson, S., and Corner, J. 2016. Challenges to seismic rehabilitation decision process in New Zealand: a focus of decision environment, International Journal of Strategic Property Management, 20(3), 305-315.

516 [18] Siddika, A., Al Mamun, M.A., Ferdous, W., and Alyousef, R. 2020. Performances,
517 challenges and opportunities in strengthening reinforced concrete structures by using FRPs- a
518 state-of-the-art review, Engineering Failure Analysis, 111, 104480.
519 [19] Mirdan, D. and Saleh, A.R. 2022. Flexural performance of reinforced concrete (RC) beam
520 strengthened by UHPC layer, Case Studies in Construction Materials, 17, e01655.
521 [20] Fehling, E., Schmidt, M., Walraven, J., Leutbecher, T., and Frohlich, S. 2014. Ultra-high
522 performance concrete UHPC: fundamentals, design, examples, Ernst & Sohn, Wiley, Berlin,
523 Germany.
524 [21] Amran, M., Huang, S.-S., Onaizi, A.M., Makul, N., Abdelgader, H.S., Ozbakkaloglu, T.
525 2022. Recent trends in ultra-high performance concrete (UHPC): Current status, challenges, and
526 future prospects, Construction and Building Materials, 352,129029.
527 [22] Shao, Y., Kuo, C.-W., Hung, C.-C. 2021. Seismic performance of full-scale UHPC-jacket-
528 strengthened RC columns under high axial loads, 243, 112657.
529 [23] Zhang, Y., Yang, J., Li, T., and Deng, M. 2022. Mechanical behavior of RC columns
530 strengthened with thin UHPC jacket under cyclic loads, Journal of Building Engineering, 49,
531 104065.
532 [24] ACI. 2017. Guide for the design and construction of externally bonded FRP systems for
533 strengthening concrete structures (ACI 440.2R-17), American Concrete Institute, Farmington
534 Hills, MI.
535 [25] Jarrah, M., Najafabadi, E.P., Khaneghahi, M.H., anbd Oskouei, A.V. 2018. The effect of
536 elevated temperatures on the tensile performance of GFRP and CFRP sheets, Construction and
537 Building Materials, 190, 38-52.

538 [26] Beavan, J., Motagh, M., Fielding, E.J., Donnelly, N., and Collett, D. 2012. Fault slip models
539 of the 2010–2011 Canterbury, New Zealand, earthquakes from geodetic data and observations of
540 postseismic ground deformation, New Zealand Journal of Geology and Geophysics, 55:3, 207-22
541 [27] Shafaei, H. and Naderpour, H. 2020. Seismic fragility evaluation of FRP-retrofitted RC
542 frames subjected to mainshock-aftershock records, Structures, 27, 950-961.
543 [28] Dahal, P. and Mullen, C. 2021. Incorporation of post-earthquake fire (PEF) and subsequent
544 aftershock for performance analysis of steel buildings, Structures, 33, 3810-3821.
545 [29] fib. 2001. Design and use of externally bonded fibre reinforced polymer reinforcement (FRP
546 EBR) for reinforced concrete structures (fib Bulletin 14), federation internationale du beton,
547 Lausanne, Switzerland.
548 [30] Padgett, J., DesRoches, R., Nielson, B., Yashinsky, M., Kwon, O-S., Burdette, N., and
549 Tavera, E. 2008. Bridge damage and repair costs from Hurricane Katrina, Journal of Bridge
550 Engineering, 13(1), 6-14.
551 [31] Benichou, N., Mostafaei, H., Green, M.F., and Hollingshead, K. 2013. The impact of fire on
552 seismic resistance of fibre reinforced polymer strengthened concrete structural systems,
553 Canadian Journal of Civil Engineering, 40(11), 1044-1049.
554 [32] ASTM. 2016. Standard practice for compressive strength of cylindrical concrete specimens
555 (ASTM C39/C39M-16a), American Society for Testing Materials, West Conshohocken, PA.
556 [33] Adamczyk, W.P., Pawlak, S., and Ostrowski, Z. 2018. Determination of thermal
557 conductivity of CFRP composite materials using unconventional laser flash technique,
558 Measurement, 124, 147-155.
559 [34] FLIR, 2019. User's manual FLIR Ex series, FLIR Systems, Inc., Nashua, NH.

560 [35] Zhou, H., Fernando. D., Torero, J.L., Torres, J.P., Maluk, C., and Emberley, R. 2020. Bond
561 behavior of CFRP-to-steel bonded joints at mild temperatures: experimental study, Journal of
562 Composites for Construction, 24(6), 04020070.
563 [36] Jahani, Y., Baena, M., Gomez, J., Barris, C., and Torres, L. 2021. Experimental Study of the
564 Effect of High Service Temperature on the Flexural Performance of Near-Surface Mounted
565 (NSM) Carbon Fiber-Reinforced Polymer (CFRP)-Strengthened Concrete Beams, Polymers, 13,
566 920.
567 [37] Altunisik, A.C., Akbulut, Y.E., Adanur, S., Kaya, A., Gunaydin, M., Mostofi, S., and
568 Mosallam, A. 2023. Evaluating the high-temperature endurance of FRP-strengthened concrete
569 using an innovative insulation system: experimental investigation, Journal of Building
570 Engineering, 73, 106444.
571 [38] Turkowski, P. 2023. Fire resistance of fire-protected reinforced concrete beams
572 strengthened with externally bonded reinforcement carbon fibre-reinforced polymers at the full
573 utilisation degree, Materials, 16, 5234.
574 [39] FEMA. 2007. Interim testing protocols for determining the seismic performance
575 characteristics of structural and nonstructural components (FEMA 461), Federal Emergency
576 Management Agency, Washington, D.C.
577 [40] Khan, M. 2002. Factors affecting the thermal properties of concrete and applicability of its
578 prediction models, Building and Environment, 37, 607-614.
579 [41] Neville, A.M. 1996.Properties of Concrete, Pearson, Essex, UK.
580 [42] Young, H.D. and Freedman, R.A. 2019. University physics, Pearson, London, UK.

581 [43] Chen, Q., Zhu, Z., Ma, R., Jiang, Z., Zhang, Y., and Zhu, H. 2021. Insight into the
582 mechanical performance of the UHPC repaired cementitious composite system after exposure to
583 high temperatures, Materials, 14, 4095.
584 [44] Gould, H. and Tobochnik, J. 2021. Statistical and thermal physics with computer
585 applications, Princeton University Press, Princeton, NJ.
586 [45] Chabay, R.W. and Sherwood, B.A. 2015. Matter and interactions, Wiley, Hoboken, NJ.
587 [46] Kim, K.Y., Yun, T.S., and Park, K.P. 2013. Evaluation of pore structures and cracking in
588 cement paste exposed to elevated temperatures by X-ray computed tomography, Cement and
589 Concrete Research, 50, 31-40.
590 [47] Wang, D., Shi, C., Wu, Z., Xiao, J., Huang, Z., and Fang, Z. 2015. A review on ultra high
591 performance concrete: Part II. hydration, microstructure and properties, Construction and
592 Building Materials, 96, 368-377.
593 [48] Lee, J., Xi, Y., and Willam, K. 2008. Properties of Concrete after High-Temperature
594 Heating and Cooling, ACI Materials Journal, 105(4), 334-341.
595 [49] Zhang, B. 2011. Effects of moisture evaporation (weight loss) on fracture properties of high
596 performance concrete subjected to high temperatures, Fire Safety Journal, 46, 543-549.
597 [50] Mishra, S. and Ayyub, B.M. 2019. Shannon entropy for quantifying uncertainty and risk in
598 economic disparity, Risk Analysis, 39(10), 2160-2181.
599 [51] Ghosh, K.K. and Karbhari, V.M. 2011. Use of infrared thermography for quantitative
600 non-destructive evaluation in FRP strengthened bridge systems, Materials and Structures, 44,
601 169-185.

602 [52] Zhang, W., Tang, Z., Yang, Y., Wei, J., and Stanislav, P. 2021. Mixed-mode debonding
603 behavior between CFRP plates and concrete under fatigue loading, Journal of Structural
604 Engineering, 147(5), 04021055.
605 [53] Baber, T.T. and Noori, M.N. 1985. Random vibration of degrading, pinching systems,
606 Journal of Engineering Mechanics, 111(8), 1010-1026.
607 [54] Yu, J., Yu, K., Shang, X., and Lu, Z. 2016. New extended finite element method for
608 pinching effect in reinforced concrete columns, ACI Structural Journal, 113(4), 689-699.
609 [55] Zhuang, Z., Liu, Z., and Cui, Y. 2019. Dislocation mechanisms-based crystal plasticity,
610 Academic Press, Elsevier, London, UK.
611 [56] Placidi, L., Barchiesi, E., Misra, A., and Timefeev, D. 2021. Micromechanics-based elasto-
612 plastic–damage energy formulation for strain gradient solids with granular microstructure,
613 Continuum Mechanics and Thermodynamics, 33, 2213-2241.
614 [57] Wang, B., Huo, G., Sun, Y., and Zheng, S. 2019. Hysteretic behavior of steel reinforced
615 concrete columns based on damage analysis, Applied Sciences, 9, 687.
616 [58] Keerthana, K. and Kishen, J.M.C. 2020. Micromechanics of fracture and failure in concrete
617 under monotonic and fatigue loadings, Mechanics of Materials, 148, 103490.
618 [59] Zhu, Y., Hussein, H., Kumar, A., and Chen, G. 2021. A review: material and structural
619 properties of UHPC at elevated temperatures or fire conditions, Cement and Concrete
620 Composites, Cement and Concrete Composites, 123, 104212.
621 [60] Ahmed, A. and Kodur, V.K.R. 2011. Effect of bond degradation on fire resistance of FRP-
622 strengthened reinforced concrete beams, Composites Part B, 42, 226-237.

623 [61] Hamad, R.J.A., Haddad, R.H., and Johari, M.A.M. 2019. New anchorage system of bars to
624 improve the mechanical performance of post-heated FRP-reinforced concrete beams,
625 Construction and Building Materials, 229, 117090.
626 [62] Baloch, W.L., Siad, H., Lachemi, M., and Sahmaran, M. 2023. Effect of high temperatures
627 on hot-bonded SCC/ECC and SCC/UHPC composite systems, Construction and Building
628 Materials, 369, 130507.
629 [63] Priestly, M.J.N. and Park, R. 1987. Strength and ductility of concrete bridge columns under
630 seismic loading, ACI Structural Journal, 84(1), 61-76.
631
632

633 **List of Tables**

634 **Table 1**. Test matrix [$^{o}F = {}^{o}C(9/5)+32$; 1 kN = 0.225 kips]

635
636

List of Figures

660 **Fig. 12**. Single-degree-of-freedom system: (a) rotational stiffness of the CF series; (b) rotational

661 stiffness of the UC series; (c) potential energy of the CF series; (d) maximum potential energy

662
663

664 **Table 1**. Test matrix [$^{o}F = {}^{o}C(9/5)+32$; 1 kN = 0.225 kips]

Beam	Strengthening	Loading	Temperature	Ultimate Load (kN)		
				Positive (P_u^+)	Negative(P_u^-)	Absolute ($\|P_u\|$)
M25NO	None	Monotonic	25°C	15.8	N/A	15.8
M25CF	CFRP	Monotonic	25°C	32.8	N/A	32.8
C25CF	CFRP	Cyclic	25°C	30.5	-30.7	30.7
C75CF	CFRP	Cyclic	75°C	21.7	-21.0	21.7
C125CF	CFRP	Cyclic	125°C	17.8	-19.9	19.9
C175CF	CFRP	Cyclic	175°C	14.9	-10.8	14.9
C25UC	UHPC+CFRP	Cyclic	25°C	32.4	-33.4	33.4
C75UC	UHPC+CFRP	Cyclic	75°C	25.4	-24.1	25.4
C125UC	UHPC+CFRP	Cyclic	125°C	21.7	-17.4	21.7
C175UC	UHPC+CFRP	Cyclic	175°C	15.6	-11.0	15.6

665 Positive = downward loading; Negative = upward loading; Absolute = maximum load in either directional loading
666
667
668

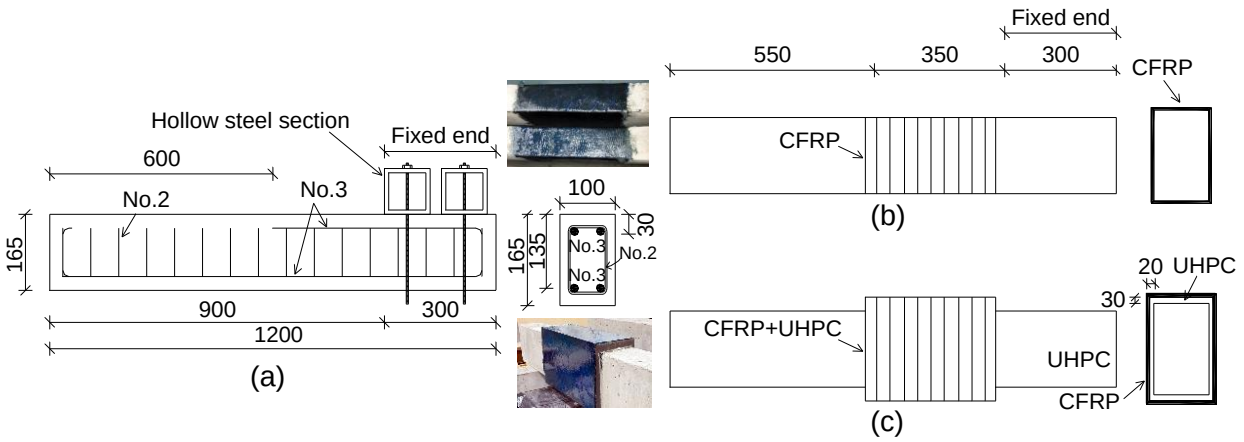

[1 mm = 0.0394 in.]

Fig. 1. Beam details (units in mm): (a) dimension; (b) strengthening with CFRP; (c) strengthening with UHPC plus CFRP

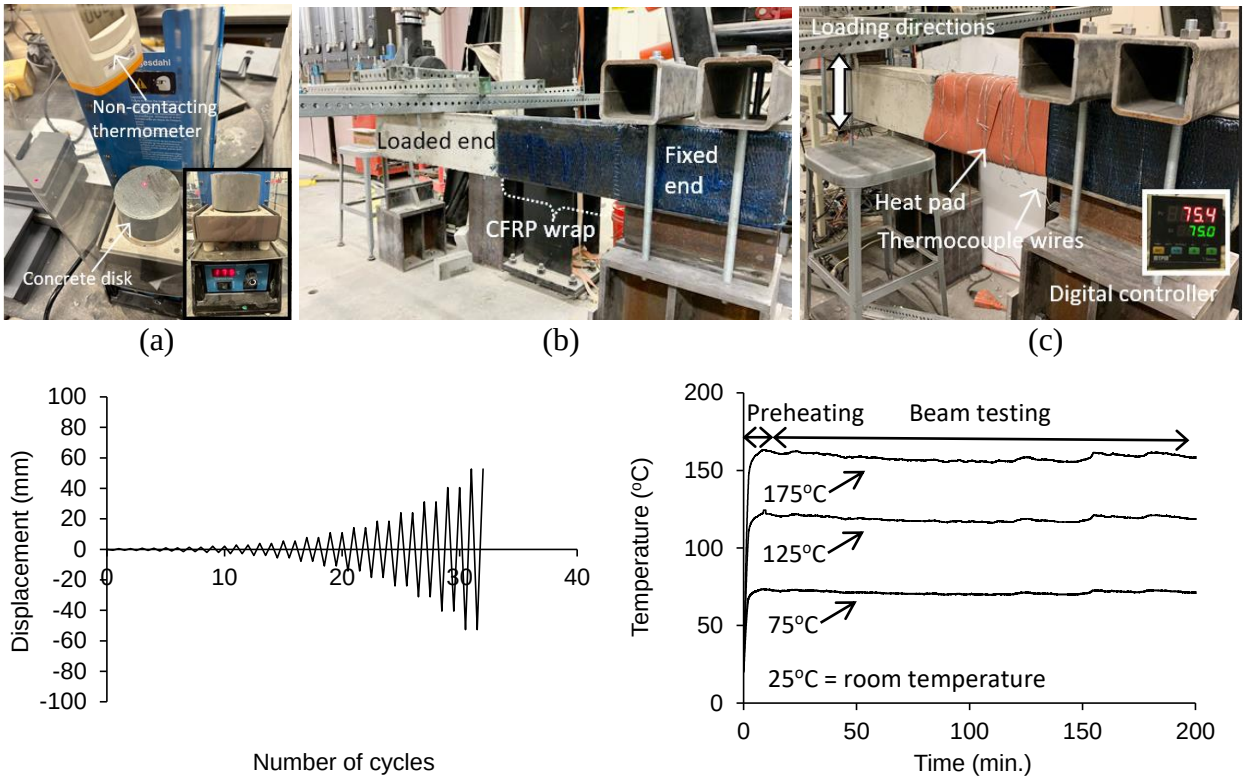

[1 mm = 0.0394 in.; °F = °C(9/5)+32]

Fig. 2. Laboratory testing: (a) thermal conductivity; (b) setup of CFRP-strengthened cantilever beam; (c) thermomechanical loading and instrumentation; (d) displacement-controlled loading scheme based on FEMA 461[39]; (e) thermocouple readings

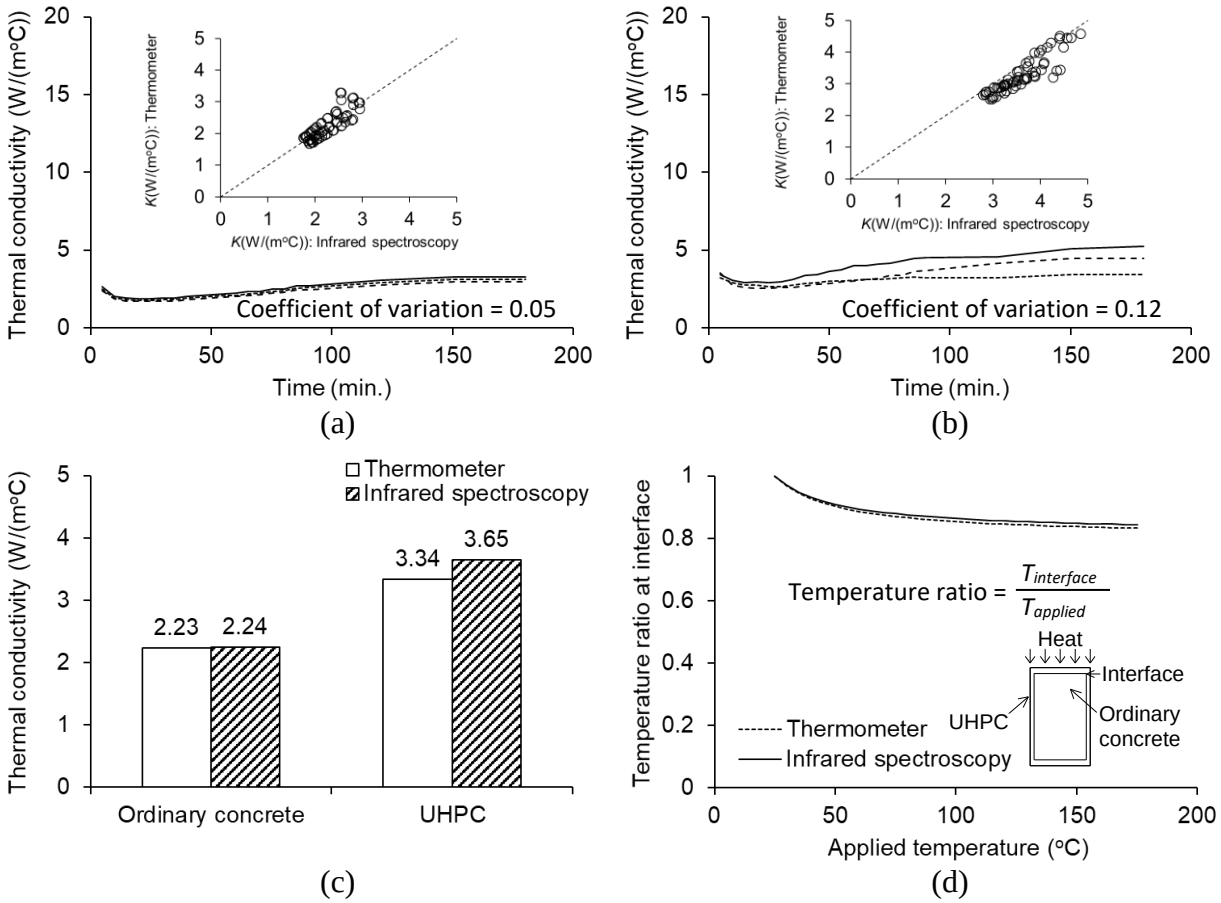

[1 W = 3.41 BTU/hr; 1 m = 3.28 ft; ^{o}F = ^{o}C(9/5)+32]

Fig. 3. Thermal conductivity: (a) ordinary concrete with non-contacting thermometer; (b) UHPC with non-contacting thermometer; (c) average conductivity of ordinary concrete and UHPC; (d) predicted temperature ratio at interface between UHPC and ordinary concrete

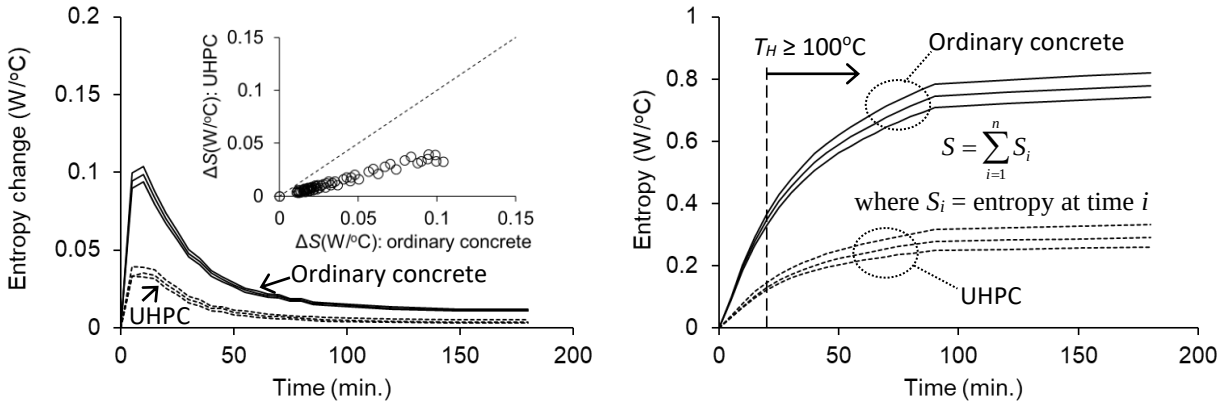

[1 W = 3.41 BTU/hr; °F = °C(9/5)+32]

Fig. 4. Entropy: (a) change with time; (b) development

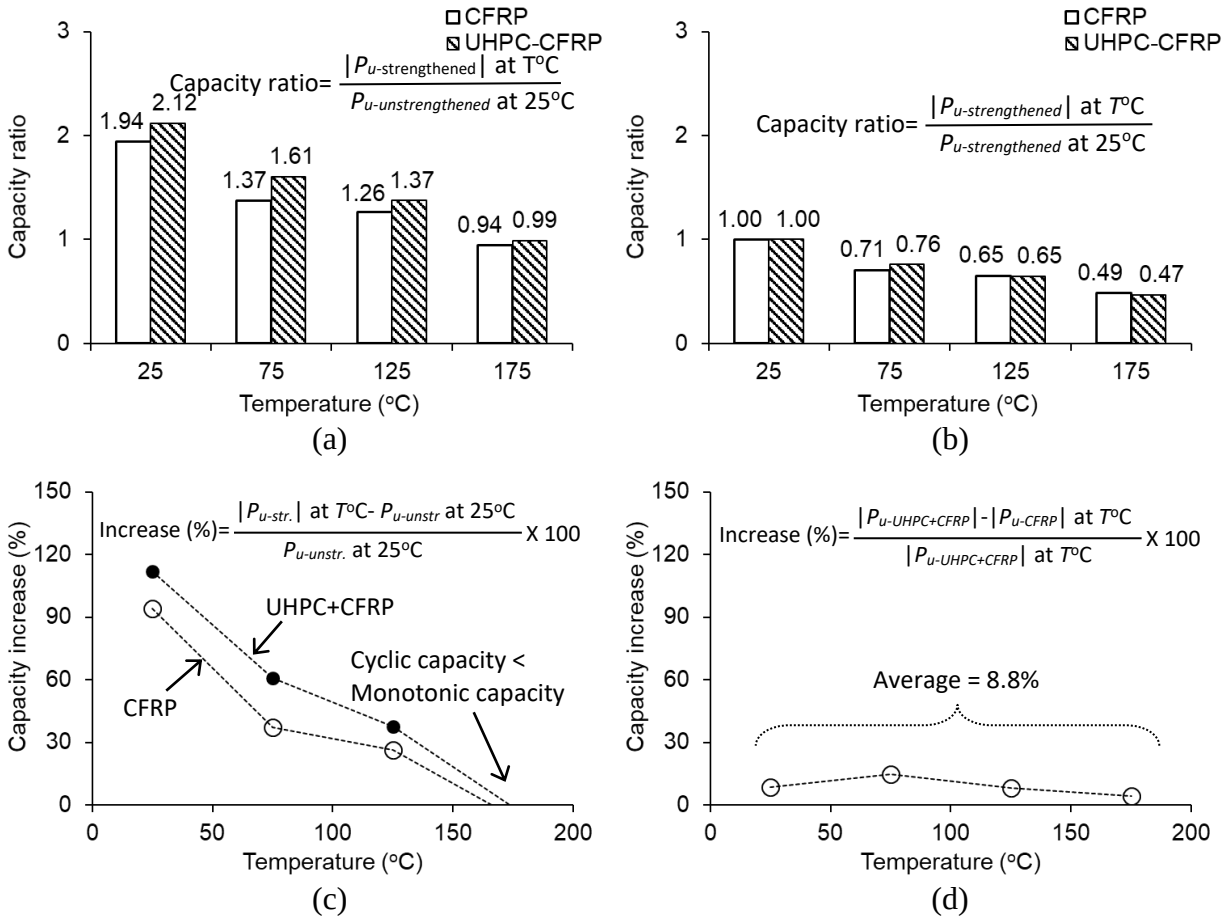

[°F = °C(9/5)+32]

Fig. 5. Capacity ratio: (a) cyclic strengthened vs. monotonic control beams; (b) cyclically loaded beams; (c) contribution of retrofit elements; (d) contribution of UHPC

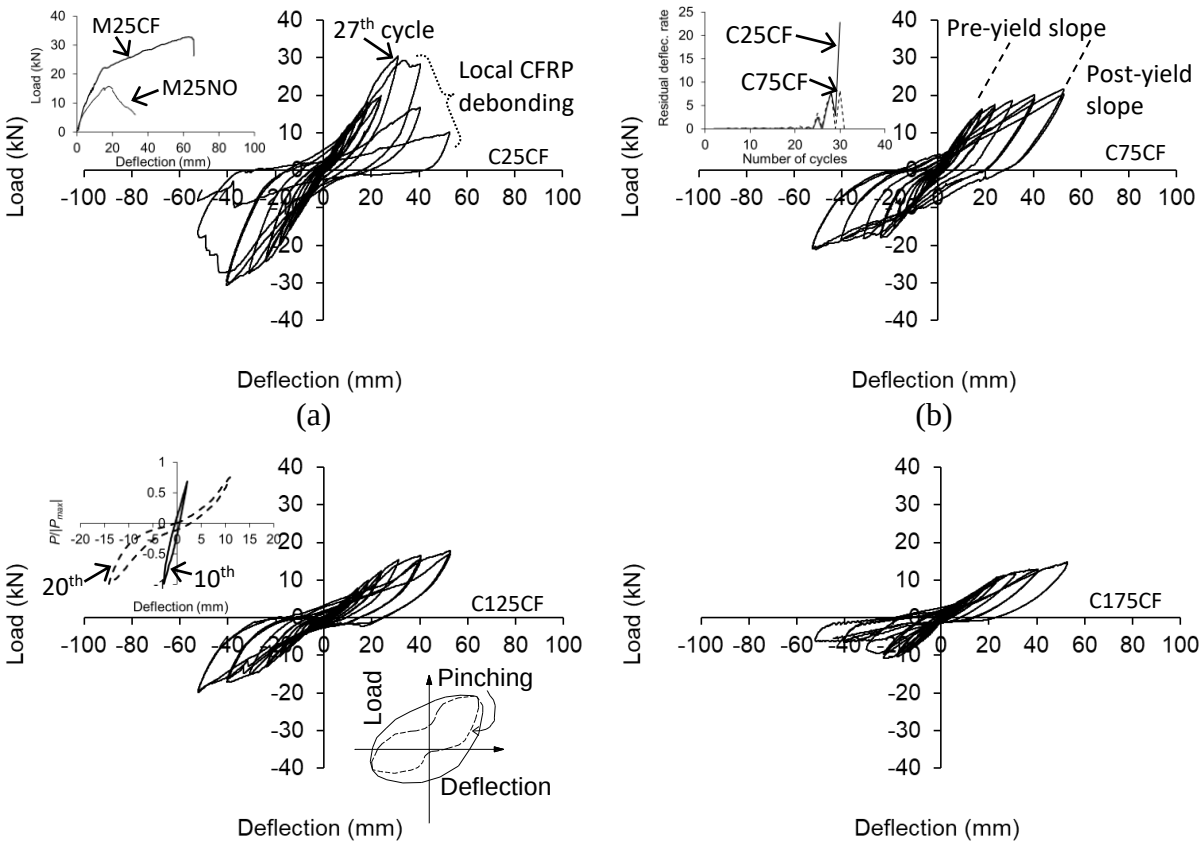

[1 kN = 0.225 kips; 1 mm = 0.0394 in.; $^{o}F = {}^{o}C(9/5)+32$]

Fig. 6. Load-deflection behavior of beams strengthened with CFRP under cyclic loading: (a) 25^{o}C; (b) 75^{o}C; (c) 125^{o}C; (d) 175^{o}C

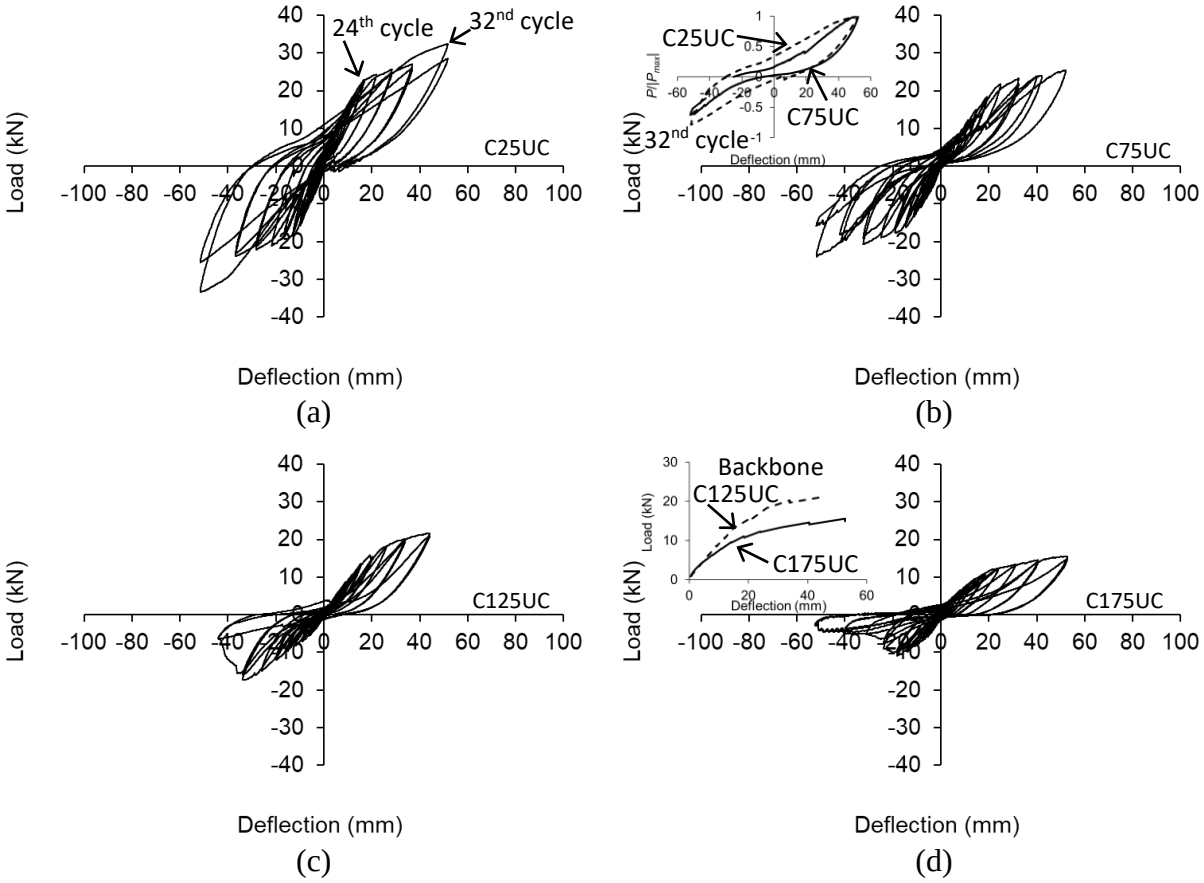

[1 kN = 0.225 kips; 1 mm = 0.0394 in.]

Fig. 7. Load-deflection behavior of beams strengthened with UHPC+CFRP under cyclic loading: (a) 25ºC; (b) 75ºC; (c) 125ºC; (d) 175ºC

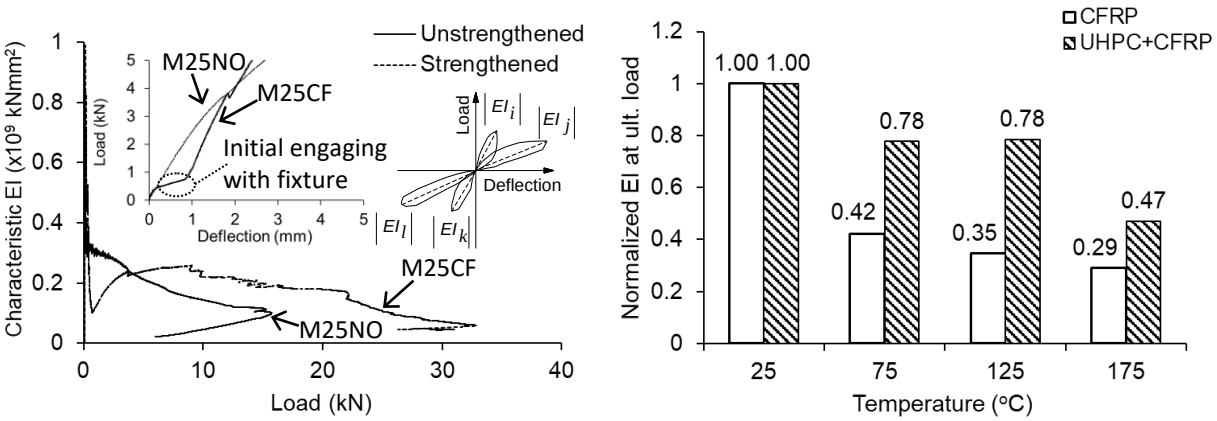

(a) (b)

[1 kN = 0.225 kips; 1 kNmm^2 = 0.00035 kip-in.^{2}; ^{o}F = ^{o}C(9/5)+32]

Fig. 8. Flexural rigidity: (a) characteristic EI under monotonic loading; (b) normalized comparison of characteristic EI under thermomechanical loading

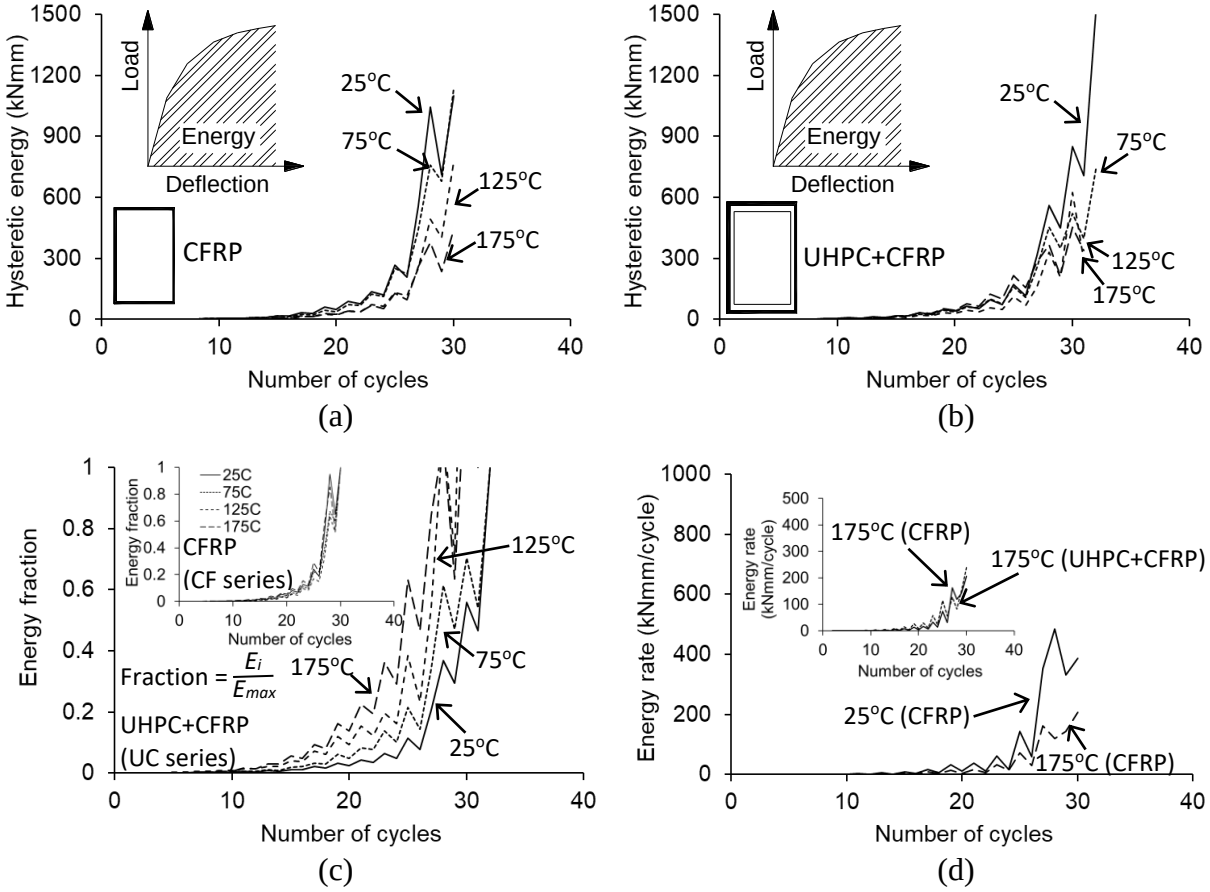

[1 kNmm = 0.0089 kip-in.; °F = °C(9/5)+32]

Fig. 9. Hysteretic energy: (a) beams with CFRP; (b) beams with UHPC+CFRP; (c) energy fraction; (d) rate per cycle

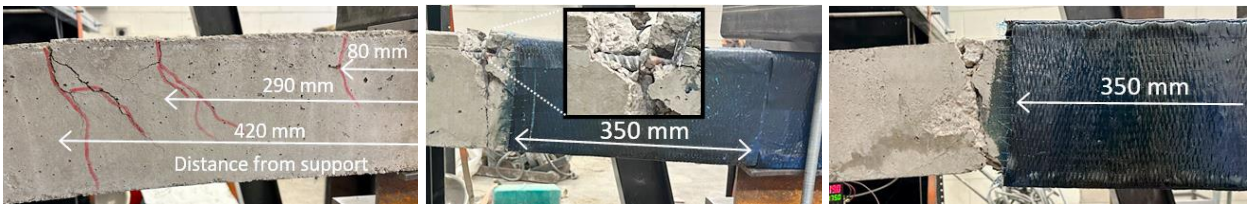

(a) (b) (c)

[1 mm = 0.0394 in.]

Fig. 10. Failure mode: (a) M25NO; (b) C175CF; (c) C175UC

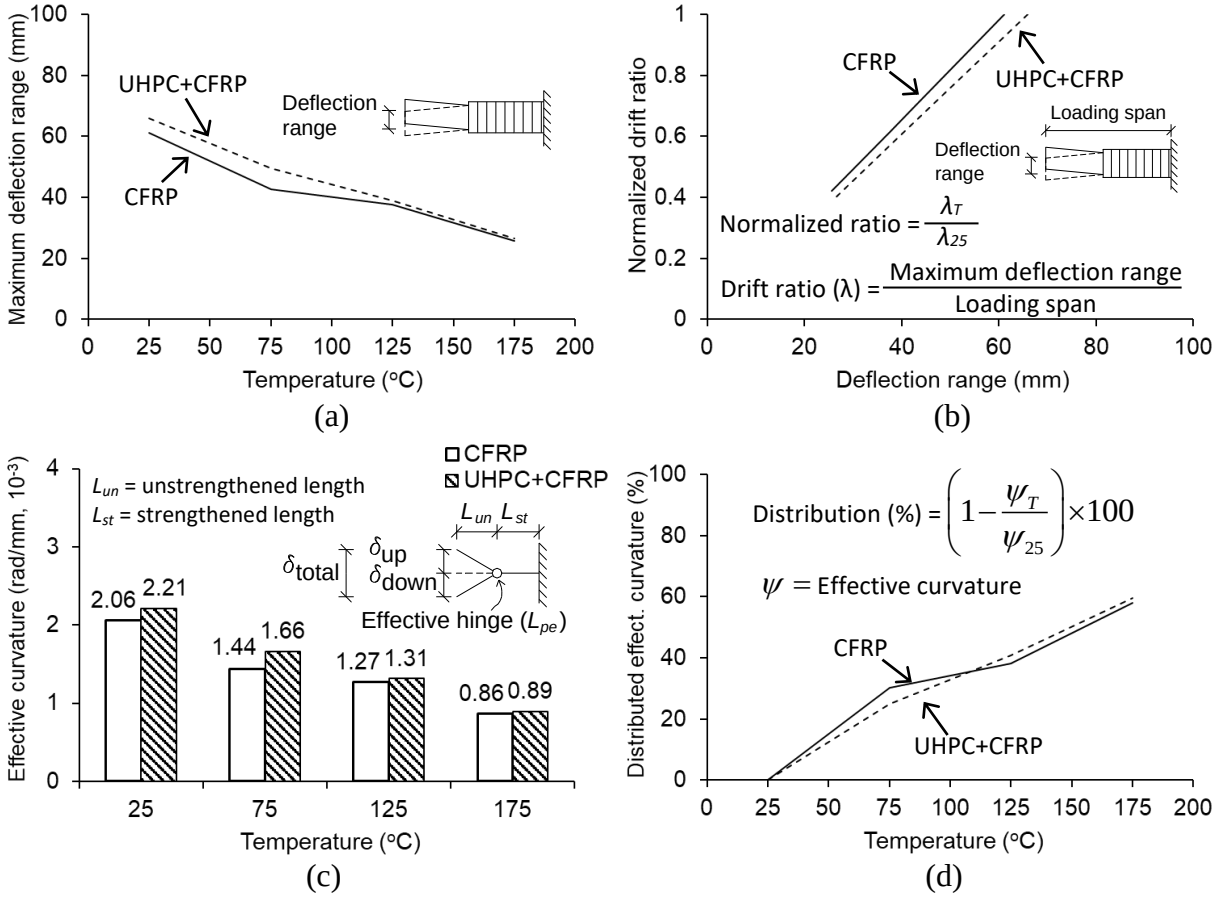

[1 mm = 0.0394 in.; °F = °C(9/5)+32]

Fig. 11. Localized deformation of strengthened beams: (a) deflection range; (b) drift ratio; (c) effective curvature; (d) distributed effective curvature

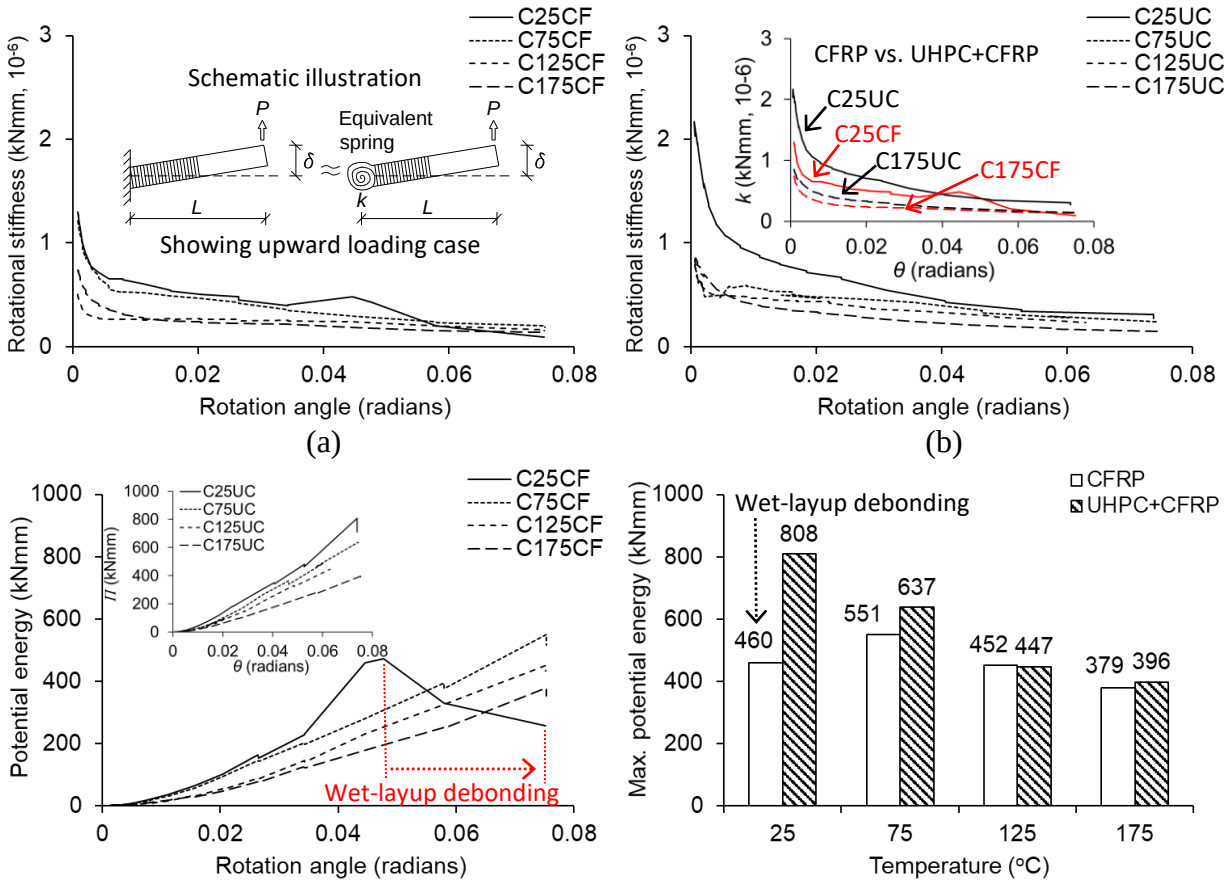

[1 kNmm = 0.0089 kip-in. ; $^{o}F = {}^{o}C(9/5)+32$]

Fig. 12. Single-degree-of-freedom system: (a) rotational stiffness of the CF series; (b) rotational stiffness of the UC series; (c) potential energy of the CF series; (d) maximum potential energy